

# **Glaciers of the McMurdo Dry Valleys:**

## **Terrestrial analog for Martian polar sublimation**

Karen J. Lewis, Andrew G. Fountain, Jeffery S. Kargel, Doug MacAyeal

**Abstract:** The surfaces of the Martian north and south polar residual caps are marked by unusual ice features: dark spiralesque troughs up to 1 km deep, 10 km wide and 300 km long appear on both ice caps, and circular pits that make up the “swiss-cheese” terrain appear on the south polar cap. Both types of features are of interest to researchers as a potential means of understanding ice composition and flow rates.

Some glaciers of the McMurdo Dry Valleys have surface features unknown elsewhere on terrestrial glaciers, including canyons over 6 km long, 100 m wide, and tens of meters deep, and basins up to 100 m across. High sublimation, dust accumulation, and very little melting, is key to their origin. These processes and ice landforms are suggested as terrestrial analogs for the sublimation behavior of Martian icecaps, where dust accumulation and sublimation are significant, but surface melting is absent.

We have developed a solar radiation model of canyon formation and have applied it to the Martian polar caps. The modeled processes do well to describe direct and reflected radiation within V-grooves, a process that may be significant in the development of the spiral troughs and swiss cheese terrain. The model fails to reproduce the low observed slopes of the Martian troughs. The grooves are too shallow, with opening angles  $\sim 165^\circ$ , compared to model predictions of  $\sim 90^\circ$ . The reason for the failure may be that we have not included creep closure, which should flatten their slopes.

## 1 Introduction

The obvious summer features on the residual polar caps of Mars are dark spiralesque markings (Fig. 1). These markings are dust-mantled troughs developed in the ice. Troughs are up to a kilometer deep and 10 kilometers wide; in the southern polar cap some are 150 km long, and in the northern polar cap up to 300 kilometers long. Seen at high resolution, the trough walls (especially the equator-facing wall) are step-like outcrops of quasi-horizontal strata or layers of alternating clean ice and dusty ice or ice-bonded dust layers. Exposure of stratification clearly indicates that these canyons have been eroded. Evidence points to deeper erosion of the canyons near the edges of the polar caps (Ivanov and Muhleman, 2000b).

There is much discussion, but no consensus, concerning the origin of Martian polar troughs. Several current theories are being explored. The first is that the troughs originate near the edges of the polar deposits and migrate toward the pole by preferential sublimation of ice from the steep, equator-facing side and accumulation on the pole-facing side, as shown in Fig. 2 (Howard, 1978; Howard et al., 1982; Fisher, 1993). Ivanov and Muhleman (2000a) used a sublimation model with no flow to reproduce, relatively successfully, the general shape of the troughs over a time span of 3 to 16 million years. The key was to provide an initial albedo contrast on the icecap surface. Fisher (1993, 2000) combines the idea of trough migration with icecap flow outward from the center; troughs migrate toward the center of the ice dome while ice flows outward from the center until the two rates are balanced. This model suggests that the spiral pattern of troughs and valleys results from the non-symmetric distribution of the ice flow centers and associated velocity fields around the pole. In addition, there have been a number of recent attempts to reproduce the troughs through sublimation and accumulation modeling. Some models which incorporate flow, (e.g. Hvidberg, 2000; Larsen, 2000) tend to have trouble keeping the troughs open over time, possibly due to the ice

rheology used for modeling. There has also been some exploration of the role of eolian erosion in maintaining the troughs (Howard, 2000).

The structural geology, geomorphology, and ice processes of individual, specific troughs are relatively unexplored. There are few published mechanisms for their initiation, and estimates of growth rates are sparse and generally only from rough parameterizations of accumulation and sublimation rates (Ivanov and Muhleman, 2000b). Existing theories for trough behavior are limited. Current theories require the troughs to be relatively recent developments, or else some as yet unexplored mechanism is required for control of their growth or for trough removal from the ice caps. None of the proposed models work as steady-state solutions where the current trough configuration is one stage in an ongoing process. Instead, the troughs need to be relative newcomers on the scene, either developed at the ice cap edge and in the process of growing inward, or recently etched into the surface via sublimation.

The goal of this paper is to use the basins and canyons found on the Canada and Taylor glaciers in the McMurdo Dry Valleys, Antarctica, as terrestrial analogs for understanding the spiral troughs of the Martian north polar cap and the swiss-cheese terrain of the Martian south polar cap. In the dry valleys, basins and canyons are formed within the ablation zones of many of the glaciers as initially small features that grow as they are carried to the glacier margin by ice flow. We propose a similar evolution on Mars starting high up on the icecap. We hypothesize that growth of the spiral troughs seen on the Martian north polar cap is initiated by locally enhanced sublimation via a perturbation in surface slope and aspect or through heterogeneous albedo due to windblown dust or grain annealing. Evidence both for small trough features and for dust deposits near the centers of the icecaps can be seen in the Mars Orbiter Camera (MOC) imagery and Mars Orbiting Laser Altimeter (MOLA) data (Howard, 2000). Once established, the features would grow via enhanced sublimation

rates on their steep, equator-facing sides, a mechanism similar to that proposed in the existing Martian scarps models and similar to the behavior of dry valleys basins and canyons. In support of this hypothesis, we present a comparison of the dry valley and Martian ice cap environment, a discussion of the morphology and development of canyons in the dry valleys, and a discussion of the Martian features.

Our hypothesis assumes that sublimation associated with enhanced solar absorption is the principal means by which grooves are excavated and maintained against closure by ice inflow. To examine this assumption a simple V-groove model, developed by Pfeffer and Bretherton (1987) to model radiation absorption within crevasses, is applied to grooves on the Martian north polar residual cap. The model calculates both incident and reflected shortwave radiation within a simplified V-groove for a specified solar azimuth. Results from this work will contribute to determining ice composition, since groove stability requires that sublimation roughly balances ice inflow. Knowledge of the composition of the Martian polar caps will help determine the history of volatile substances (water and carbon dioxide) in the Martian atmosphere and on the Martian surface.

In addition to the trough features seen on both Martian ice caps, MOC has recently returned images of strange features on the south polar residual cap that have been termed the “swiss cheese” terrain (Fig. 3) (Malin and Edgett 2001, Malin et al. 2001). Byrne and Ingersoll (2000) have attributed the origin of this terrain to ablation via sublimation of CO<sub>2</sub> ice. The circularity of pits probably is a result of sublimation at high southern latitude where solar elevation is nearly constant throughout the day and, therefore, ablation on the walls of depressions is roughly radially symmetric. The formation of the swiss-cheese pits takes place on century time scales, the same time scales as formation of canyons and basins in Antarctic ice glaciers. Significant interannual changes have been

observed (Malin et al. 2001). The morphologies present within the swiss-cheese terrains are quite varied and point out the possibility that they consist of layers of multiple ices (H<sub>2</sub>O, CO<sub>2</sub>, and CO<sub>2</sub> clathrate are all likely). Less volatile ice layers—water ice perhaps—may form mesa tops and hole bottoms, with more volatile ice layers in between which can rapidly ablate outward from an initial point, as is postulated in Thomas et al., 2000.

As with the polar troughs, further insight into the working of these features can be gleaned from comparison with the basins seen on dry valley glaciers. We propose that these features are the result of sublimation of the surface in the absence of effective wind removal of debris. Sheltered conditions within the basins may aid retention of debris, as seen in the dry valley basins. The first areas of the swiss-cheese terrain to become free of winter dry-ice snows—leaving dusty, annealed layers of dry ice behind—are scarps, as expected. The snow-free scarps should have a large effect on the local radiative environment, as may be evidenced by the moats commonly seen fringing the foot of most scarps, though other possible explanations for the moats have also been put forward (Thomas et al., 2000).

## **2 The physical environment: Antarctic dry valleys vs. Martian polar regions**

Though very different environments, there are enough critical similarities between the Antarctic dry valleys and the Martian polar regions to allow for fruitful comparison between the two. Both are cold, dry regions where energy for ablation is limited, accumulation and sublimation rates are relatively small, and ice flow speeds are low. In these regions, strange topography can be etched into ice surfaces as a result of dominance of sublimation and differential ablation rates.

Table 1 presents a number of physical environmental parameters for both regions. With the exception of accumulation and ablation of CO<sub>2</sub> ice, which doesn't exist under ambient surface conditions on earth, polar processes on Mars occur more slowly than on Earth. Atmospheric pressure and water vapor pressure are several orders of magnitude smaller; accumulation and ablation rates for water ice are several orders of magnitude smaller; the ice is much colder, resulting in a much smaller range of probable flow speeds. Gravity is about a third that of earth and solar radiation a little less than half that of earth. Length of day and obliquity are among the few physical parameters that are nearly equal. However, the ratios of accumulation vs. sublimation for water ice are similar; sublimation is up to one order of magnitude greater than accumulation. Similarly, the ratio of accumulation to flow speed is about 10<sup>2</sup> and of sublimation to flow speed is about 10<sup>1</sup> to 10<sup>2</sup> (see Table 1). This similarity may be part of the key to understanding why large roughness features form both in the McMurdo Dry Valleys and on Mars in spite of environmental differences.

Controls on the rate of sublimation are somewhat different on Earth and Mars. In the Earth atmosphere sublimation is predominantly a function of the vapor pressure difference between the surface and the air, and of the speed of turbulent dispersion of the air. Consequently, equations for sublimation incorporate the vapor pressure gradient, wind speed, as a measure of turbulence, and buoyancy effects. The latent energy flux,  $Q_E$ , for earth conditions can be written as:

$$Q_E = -u^* k_o z \left( \frac{0.622 \rho_i}{P} \right) \frac{\partial e}{\partial z} L_s \quad \text{Equation 1}$$

where  $u^*$  is a characteristic scale of wind speed,  $k_o$  is the von Karman constant,  $z$  is the height at which wind speed and vapor pressure are measured,  $\rho_i$  is the ice density,  $P$  is atmospheric pressure,

$\frac{\partial e}{\partial z}$  is the gradient of atmospheric vapor pressure with height, and  $L_s$  is the latent heat of sublimation

(Paterson, 1994).  $u^*$  is written as:

$$u^* = \frac{uk_o}{\ln\left(\frac{z}{z_o}\right)} \quad \text{Equation 2}$$

where  $u$  is the average wind speed, and  $z_o$  is the surface roughness parameter. Since sublimation on Earth is driven by vapor pressure gradients and wind, only in extreme conditions will sublimation be limited by energy availability. (Sublimation cools the surface until the change in vapor pressure gradient reduces sublimation rates to match energy availability.) This type of energy limitation of sublimation does not occur in the dry valleys during the summer. Consequently, for our purposes here sublimation on Earth can be considered to be entirely forced by wind and vapor pressure gradients.

For Mars, due to the low atmospheric pressure (<20 mbar), the dominant process controlling water vapor flux is natural convection. Water vapor is more buoyant in the Martian CO<sub>2</sub> atmosphere than it is on earth (Toon et al., 1980). At the same time, forced convection via wind and vapor pressure gradients plays a relatively small role. For Martian conditions the vapor flux is written with two equations (Toon et al., 1980), the first for turbulent transfer as a result of winds, and the second for turbulent transfer as a result of natural convection:

$$Q_{E1} = 0.002\rho_w u L_s \quad \text{Equation 3}$$

$$Q_{E2} = 0.017\rho_w D \left[ \left( \frac{\Delta\rho}{P} \right) \left( \frac{g}{\nu^2} \right) \right]^{1/3} L_s \quad \text{Equation 4}$$

In these equations  $\rho_w$  is the water vapor density,  $D$  is a diffusion coefficient for H<sub>2</sub>O in a CO<sub>2</sub> atmosphere,  $P$  is atmospheric pressure,  $\frac{\Delta\rho}{P}$  relates water vapor pressure to atmospheric pressure,  $g$  is gravity, and  $\nu$  is the viscosity of CO<sub>2</sub>. Values for the constants can be found in Toon et al. (1980).

These equations are very similar to the sublimation equations used by others (e.g. Ingersoll, 1970; Haberle and Jakosky, 1990). Of these two terms,  $Q_{E2}$  generally dominates over  $Q_{E1}$ . This means the primary control on sublimation lies in  $Q_{E2}$  in the  $\frac{\Delta\rho}{\rho}$  term, which is governed by surface temperature. Surface temperature is governed primarily by energy absorption. Thus Martian sublimation is driven primarily by energy absorption at the surface, which implies that slope, aspect and albedo enhancement of energy absorption will directly increase ablation.

An important similarity between the dry valley glaciers and the Martian polar caps is that both regions are energy limited. In the dry valleys, temperatures are typically below freezing and much of the ablation is due to sublimation resulting from the persistent high winds, which greatly reduces or eliminates energy available for melt (Lewis et al., 1998). Therefore, if energy absorption is enhanced on a surface, for example via slope, aspect or albedo, that energy will be primarily converted to melt and the surface will experience significantly more ablation. For the same amount of energy, melt is about 10 times more efficient than sublimation at removing ice, so only a small amount of “extra” energy devoted to melt is needed to make a large impact on local ablation.

On the Martian polar caps, energy availability limits sublimation much as energy availability limits melt in the dry valleys. Temperatures do not reach the melting point on the Martian polar caps. The altitude of the south polar cap is such that barometric pressure is less than the triple-point pressure, so even with a remarkable and unlikely coincidence of conditions that could allow the melting point to be attained, the ice would first sublimate. Local slope, aspect and albedo do have dramatic effects enhancing local sublimation rates on the Martian polar caps much the same as they allow increase melt in the dry valleys. When coupled with the longer time scales over which features form on Mars, enhancements in sublimation are enough to form sublimation pits or canyons. On Earth, it is the factor of 10 difference between melt and sublimation that allows canyon and pit

formation. Through increased melt, the dry valleys channels on Taylor Glacier, which are roughly 10 m x 100 m x 1 km in size, form in about 1000 years (see section 3). On Mars, features 1 km x 10 km x 100 km may form over an estimated time span of  $5 \times 10^7$  years (assumes ice flow of  $10^{-2}$  m/year for a distance of 500 km, the radius of the ice cap). So, we have a factor of  $5 \times 10^4$  more time on Mars to form features 100 times larger. This implies that processes can be up to 500 times slower on Mars than on Earth and still produce troughs of the sizes seen in the residual polar caps.

### **3 Glacier surface morphology in the McMurdo Dry Valleys, Antarctica**

The basins and canyons found on the dry valley glaciers appear to form as a result of three principal environmental factors. (1) The glaciers are frozen to their beds and move comparatively slowly. Features in the ablation zone of the glaciers have hundreds to thousands of years to develop. (2) The environment is dry and windy and deposits of dust and sand (either through eolian processes, medial moraines, or rock avalanches) are ubiquitous on the glaciers ( $0.5-1 \text{ g/m}^2/\text{year}$ ). The debris melts into the ice, if only a short distance. Generally meltwater is absent or insufficient to wash the sand and dust off the glacier. (3) The environment is energy poor. Temperatures are typically below freezing and there is relatively little incoming energy, about  $40 \text{ Wm}^{-2}$  on average over the summer season (Lewis et al, 1998). The low levels of available energy, coupled with the cold, windy conditions, results in very little melt on the glacier surfaces. What little energy is available goes primarily to sublimation. As a result, small changes in energy receipt on the glacier surface as a result of albedo, slope, and aspect greatly affect melt production (Lewis et al., 1998).

The basins on the dry valley glaciers appear to nucleate around debris. Isolated patches of debris form ~30 cm deep cylindrical holes, “cryoconite holes”, in the glacier surface (Mueller et al., 2001; Wharton et al., 1985). These holes vary in radius from a few centimeters to over a meter. At

small radii the holes retain an ice cover and appear to grow very slowly. At radii  $> 0.5$  m the holes begin to lose their ice covers. At this point, if debris and meltwater within the holes can drain, the holes can rapidly deepen and widen (up to  $\sim 0.50$  m per summer in both depth and width – Lewis, 2002). In the process, the holes take on an asymmetric geometry. The pole-facing wall develops into a shallow pole-facing slope due to shading while the equator-facing wall remains vertical and melts back relatively rapidly (Fig. 4). A similar process applies to the long channels or canyons, such as on Taylor Glacier, but the source of debris is medial moraines that originate at the confluences of the glacier tributaries (Fig. 5). Basin and valley formation therefore requires both the initial presence of debris and the removal of debris and meltwater when the feature reaches a critical size, and results in a feature geometry that enhances solar radiation absorption in some locations and reduces solar absorption in others.

The Taylor Glacier canyons (Fig. 5 and Fig. 6, right-hand image) appear to start about 3 km from the glacier terminus as approximately 1 m deep grooves. These grooves, initiated by medial moraine debris, grow as they are carried down-glacier by ice flow. Ice speed is 4 to 7 m/year, so the 3 km distance from the point of canyon initiation to the glacier terminus represents 400 to 750 years of evolution. At the terminus, the grooves have become 10 to 20 m deep chasms in the glacier surface, formed by differential ablation rates and modified by water flowing within the canyon. The canyon width initially varies, with wide pool-like features separated by relatively narrow passages. At some point, these features vanish and the width to depth reaches a nearly constant value.

The Canada Glacier basins are more randomly distributed than the canyons on Taylor Glacier because they nucleate around debris patches (Lewis, 2002). Due to their more random distribution, the basins seem to function more as isolated features, each growing at its own rate. Timescales for

basin growth on Canada Glacier are 400 to 3000 years (ice flow rates of 1 to 8 m/year over a distance of up to 3 km).

#### **4 Martian icecaps – their climate and behavior**

Current consensus is that the composition of the Mars north polar residual cap is water ice, with only a seasonal CO<sub>2</sub> frost that completely sublimates during the summer (Clifford et al., 2000). However, there are alternate possibilities that would include CO<sub>2</sub> clathrate and/or dry-ice at depth (Mellon 1996, Ross and Kargel 1998, Kargel and Lunine 1998, Kargel et al. 2000). The composition of the south polar cap is less well understood, but accumulating evidence points toward a form of CO<sub>2</sub>/H<sub>2</sub>O clathrate or some layering of CO<sub>2</sub>, H<sub>2</sub>O and CO<sub>2</sub> clathrate ices (Jakosky et al., 1995; Kargel and Lunine 1998; Thomas et al., 2000). On both caps, air and surface temperatures, at the current obliquity, do not reach, or come close to attaining, the melting point of H<sub>2</sub>O. Winter temperatures on both caps drop to 148 K, allowing the deposition of CO<sub>2</sub> frost. Summer high temperatures for the northern cap and outlying southern polar layered deposits are about 205 K (Kieffer et al., 1976, 1992, Jakosky et al. 2000), resulting in the sublimation of the winter accumulation of CO<sub>2</sub> frost as well as some portion of the water ice of the cap. This has been seen in the Mars Atmospheric Water Detection (MAWD) data (Farmer et al., 1979) which shows enhanced water vapor over the north pole in summer. On the south polar cap, summer temperatures do not always rise measurably above the dry-ice frost point (about 148 K), so that carbon dioxide frost, deposited during the fall and winter, may not completely sublime during the summer season (Kieffer 1979; Jakosky and Haberle, 1992). The distinct morphologies of the two polar caps also support a different surface ice composition. Since temperatures stay well below the melting point for both caps, ablation will only occur via sublimation and wind erosion. Since sublimation increases

with temperature (Jakosky et al., 1993; Ivanov and Muhleman, 2000a), ice slopes that face the sun or are dust covered will warm and sublimate faster. This results in the formation of accentuated slopes or depressions that receive yet more energy, leading to a positive feedback.

Sublimation is not the only process controlling trough geometry. Because the ice cap is so thick, and because the troughs are so deep, trough location and shape will be affected by ice thickness and rheology and trough closure by ice flow will probably be significant. The north polar cap rises approximately 3 km over the surrounding terrain. Zuber et al. (1998) calculated an icecap thickness of roughly 3.5 to 4 km. For the southern ice cap Schenk and Moore (2000) estimate the south polar cap to be a broad convex dome approximately 500 km in diameter with a maximum height of 3 km above the surrounding plains.

Such thick ice will flow (Budd 1986, Greve 2000). If the caps were at the measured surface temperatures throughout they would flow very slowly, but the ice is probably warmer at depth due to geothermal heating. Larsen and Dahl-Jensen (2000) calculate that the basal temperature of the Martian north polar cap may be similar to that of terrestrial ice caps, i.e., close to the freezing point, implying that flow speed will be governed primarily by deformation at the base and may be roughly the same as terrestrial ice caps of similar dimensions. Flow closure of the troughs, however, would be slower than terrestrial conditions since the near-surface ice in the cap will be closer to mean annual temperatures.

Flow on the south polar cap is more difficult to assess since ice composition is still unknown. Pure CO<sub>2</sub> ice is significantly softer than water ice, which, combined with the overall cap geometry, suggests that the south polar cap cannot be pure CO<sub>2</sub> (Nye, 2000). H<sub>2</sub>O-CO<sub>2</sub> clathrate, however, is much stiffer than pure water ice (Durham et al., 2000). At south polar thickness and temperatures, a pure clathrate ice cap might flow so slowly as to be virtually immobile. Consequently, understanding

the role of flow closure in the overall geometry of the south polar troughs will require significantly more study.

## **5 Proposed evolution of the Martian north polar troughs**

The troughs cutting the north polar residual cap (Fig. 8) vary greatly in depth. The shallowest troughs measured are about 100 m deep; the deepest troughs are about 1 km deep, cutting through the polar cap almost to the level of the surrounding plains. The troughs strike about 20 degrees north of west (Howard, 2000), which gives them their distinctive spiral look, and are steeper on the equator-facing walls than on their pole-facing walls (Ivanov and Muhleman, 2000b). Equator-facing walls range from 1 to 10 degrees slope; pole-facing walls range from less than a degree to about 6 degrees slope. In general, wall slope seems to increase with wall height, so that the deepest grooves also have the steepest sides (Ivanov and Muhleman, 2000b). Similarly, on the south polar residual cap troughs range in depth from about 100 m to over 800 m, with equator-facing walls ranging from 1 to 9 degrees slope and pole-facing walls ranging from less than 1 to nearly 4 degrees slope (Ivanov and Muhleman, 2000b).

Assuming the Martian ice cap troughs result from a series of events similar to those giving rise to the basins and canyons on the dry valley glaciers, we believe that the Martian troughs are primarily radiation generated and maintained features. They are initiated high on the ice caps by some combination of small-scale surface roughness and dust. The small-scale roughness may be snow dunes (Howard, 2000) or something akin to the “cottage-cheese” terrain photographed by MOC. This terrain is characterized by pitting of relatively regular width, varied length and connectivity, and depths of about two to several meters, and seems to cover most of the north-polar residual cap (Thomas et al., 2000; Malin and Edgett 2000, Malin et al. 2001). Either pitting or snow

dunes will serve to trap dust, thereby lowering surface albedo and increasing energy receipt. Dune and pit geometry will also affect energy receipt as local slope and aspect increase or decrease incident radiation.

As ice on the sides and floor of the dunes and pits sublimates, dust frozen into the ice will be freed. Accumulation of a thin layer of dust will increase ablation until the layer thickens and begins to insulate the ice. In a similar manner, ablation in the basins and canyons of the dry valley glaciers increases for thin debris cover and greatly decreases when the cover thickens sufficiently to insulate the ice. In the dry valleys, flowing water removes the debris from the ablation features. Current estimates of dust content of the Martian ice range from 50% to less than 1% by volume (Clifford et al., 2000). This is sufficient to reduce the albedo and increase sublimation in the early stages of feature formation. However, sublimation of 1-10 m of ice will release ample dust to build up an insulating layer. Larger features will only form on the Martian residual caps in areas where wind transport can evacuate the excess dust. The wind will also aid in linking small basins and depressions into elongate features much as water links basins into canyons on Taylor Glacier. This suggests that mature Martian troughs form in geometries that optimize both radiation receipt and wind transport. This conclusion is supported by Howard (2000), who notes that the troughs strike at an angle 20 degrees north of west, intermediate between the direction of greatest radiational loading and an orientation normal to the katabatic wind flow.

The need for wind removal of the dust freed by ice sublimation may also explain the trough spacing on the ice caps. The troughs appear to be spaced fairly regularly at 20 to 70 km intervals. The ice between troughs forms a gentle bulge with a divide roughly halfway between, as can be seen in MOLA data. We hypothesize that this is due to some channeling of the katabatic winds as they flow off the ice cap, possibly dictated in part by polar atmospheric waves. If the natural modes of the

wind form some quasi-equally spaced banding, this in turn would favor dust deposition in or removal from roughness features at the center of those bands, leading to both faster development of roughness features in those regions and the linkage of those features downwind. This would further channel the wind leading to a positive feedback loop and fairly regularly spaced mature troughs.

Once initiated, the troughs will probably collect more debris on their floors than on their walls, leading to faster downward growth than lateral growth. As a result, the walls will steepen over time as the trough becomes deeper. This is supported by Ivanov and Muhleman's measurements that indicate deeper troughs have steeper walls (Ivanov and Muhleman, 2000a). Exposed dust banding in the equator-facing trough walls, seen in MOC imagery, indicates that the equator-facing walls experience net ablation. The pole-facing walls receive less radiation than the equator-facing walls as a result of their slope and aspect and will therefore be cooler. Sublimation on the pole-facing walls will be lower or non-existent. MOC imagery suggests the pole-facing walls may experience net accumulation since the debris banding in the ice seen on the equator-facing walls is not always visible on pole-facing walls.

## **6 Radiation receipt within the Martian north polar troughs – Why so shallow?**

The enhancement of solar absorption derived from V-groove geometry results from a geometrical “greenhouse” effect that stems from two physical principles. First, when the solar zenith angle is large, common at polar latitudes, an inclined surface oriented toward the equator gathers more sunlight. Therefore, equator-facing slopes on terrestrial and Martian ice surfaces alike become steeper than opposing faces, which are shadowed, because they receive more energy and therefore have higher ablation rates. Second, outgoing reflected light from natural snow and ice surfaces can be treated as diffuse and varies with the cosine of the incidence angle of the incoming beam. A

portion of the diffuse reflected energy is directed toward the opposing wall where it is reflected again. The multiplicity of reflections associated with the diffuse radiation leads to greater absorption because some fraction of the incident energy is absorbed with each reflection (Fig. 8).

The radiative regime of an idealized Martian trough with perfect “V” geometry is computed following Pfeffer and Bretherton’s (1987) work on crevasses on terrestrial glaciers acting as solar radiation traps. We chose parameters to represent typical valleys on the Martian northern ice sheet (Table 2), which are derived from a visual analysis of the MOLA transects and valley profiles. We ignored secondary effects such as angular heterogeneity in the absorptivity of an icy surface and the effects of “far field” topographic patterns, such as the general slope of the ice sheet and the effects of distant ice structures that may cast shadows or radiate energy on points within the groove. Nor is small-scale roughness on the sides of the groove, such as the “stair-step” topography found in the dry valleys, considered, though there is some evidence in the MOC imagery that stair-step topography may occur within the Martian grooves.

As illustrated in Fig. 8, variables  $x$  and  $y$  are non-dimensional coordinates that describe distance along each of the two walls from an origin at the bottom of the “V”. The  $y$ -coordinate is associated with the wall that faces the sun, the equator-facing wall of the groove. The coordinate axes are separated by the angle  $\gamma$ , the V-groove opening angle. Thus the coordinate axes are not Cartesian. The variable  $\Psi$  is the angle between the direct solar beam and the line that bisects  $\gamma$ . The angle  $\Psi$  is related to the solar zenith angle, which depends on the time of year and time of day, as well as other long-term variables such as the planet's obliquity.  $\Psi$  also depends on the inclination of the V-groove's line of symmetry from the vertical. For typical grooves on the ice sheets of Mars, the equator-facing wall is steeper than the opposing wall by about a factor of 2 and ranges in slope from 4 to 10 degrees. Thus the line of symmetry is typically inclined toward the equator by 1 to 4 degrees.

## 7 Results and discussion

Fig. 9 shows the results for a typical Martian groove, where  $\gamma \sim 165^\circ$  (the equator-facing wall is at a 10 degree slope, the pole-facing wall at a 5 degree slope) and where englacial and surficial debris causes the reflectivity to be much reduced (we use  $\rho = 0.3$  on the equatorial-facing wall and  $\rho = 0.4$  on the poleward-facing wall). The calculation displayed in Fig. 9 represents the circumstances encountered at  $80^\circ$  N at noon on the summer solstice (for a groove that extends east to west).

The most important result, shown in Fig. 9, is that energy absorption on the sun-facing wall is significantly enhanced over the energy absorption on a flat, horizontal surface. The sun-facing wall, because it is inclined toward the incoming solar beam, absorbs about 140% of the energy that a flat, horizontal surface would absorb. The enhancement of incoming energy is analogous to that observed for the basins and canyons on the Antarctic dry valleys glaciers. Reflected radiation accounts for 2% of the total absorbed radiation. The sun-opposing wall absorbs about 80% of that on a flat, horizontal surface. On the sun-facing wall reflected radiation accounts for less than 1% of the total.

The low values for reflected radiation imply that the large opening angles of the Martian grooves don't allow the groove walls to “see” each other. This implies that re-radiated longwave radiation absorption will also be low. These results show that a relatively simple parameterization of incoming radiation can be used for the grooves, such as the straight cosine dependence of Ivanov and Muhleman (2000a) Equation 6. Omitting multiple reflections only incurs an error of about 2% in the radiation calculations.

The radiation regime is computed for  $\gamma = 60^\circ$ , the approximate opening angle of the Taylor Glacier canyons (the equator-facing wall is vertical, the pole-facing wall is at 30 degrees), to show

the sensitivity to groove opening angle (Fig. 10). At this opening angle, the pole-facing wall and the lower portion of the equator-facing wall are both shadowed. The lower portion of the equator-facing wall absorbs up to  $20 \text{ Wm}^{-2}$  of shortwave radiation because of reflection off the pole-facing wall. The pole-facing wall receives up to  $100 \text{ Wm}^{-2}$  from reflection off the equator-facing wall. Comparison with Fig. 9 shows that as  $\gamma$  is reduced the overall efficiency of the groove in capturing solar radiation becomes greater relative to that of a flat, horizontal surface. The incident radiation on the equator-facing wall is strongly enhanced because the wall more directly faces into the sun, and the reflected radiation component of the total absorbed radiation is large due to the narrow opening angle of the groove.

The variation of absorption with opening angle prompts us to speculate on the possible time-evolution of Martian grooves. In model runs for grooves with  $\gamma < \sim 60^\circ$ , the energy is strongly concentrated near the top of the groove. If allowed to generate ablation through sublimation, this energy concentration will cause the groove to widen near its top, and thus cause  $\gamma$  to increase. In model runs with  $\gamma > \sim 90^\circ$ , the radiation absorbed by the two walls becomes more or less uniform over the length of the walls, as is the case displayed in Fig. 9. Further sublimation is then expected to enlarge the groove, maintaining its depth to width ratio, and tilt its axis of symmetry toward the sun. Thus, an opening angle of  $\sim 90^\circ$  or more appears to be “optimum” in the sense that once it is achieved, the groove will both deepen and widen while maintaining a constant shape (i.e., a constant  $\gamma$ ).

However, if  $\gamma \sim 90^\circ$  is “optimum”, why do the troughs on the Martian residual caps have opening angles of  $165^\circ$ ? On Taylor Glacier the canyons can be characterized as grooves with an opening angle of  $60$  to  $90^\circ$ . In particular, the pole-facing walls slope quite consistently  $30$  to  $35^\circ$ , an angle that serves to minimize the incoming direct solar beam. This is clearly not the case on the

Martian icecaps where the pole-facing walls slope at angles of 1 to 6°. Similarly, the slopes seen on the equator-facing walls do not maximize incoming radiation, unlike in the dry valleys of Antarctica where equator-facing slopes are near vertical. This suggests that on Mars some mechanism, such as closure by flow, is at work to keep the slopes relatively shallow. If so, quantifying radiation receipt and sublimation within the troughs may allow us to estimate ice flow rates.

## **8 Some speculations on the origin of the “Swiss cheese” terrain**

Thomas et al. (2000), Byrne and Ingersoll (2000), Malin and Edgett (2000) and Malin et al. (2001) attribute the basins in the south polar “swiss-cheese” terrain to sublimation. This would explain their circular shape, steep walls, and the appearance in MOC imagery that they grow outward from an initial point, pass through a stage where they overlap in places and leave oddly shaped mesas in others, and ultimately leave behind a new surface, flattened at the level of the basin floors. However, if sublimation and high latitude were the only factors required for basin growth, we should also see swiss-cheese terrain on the north polar cap. Since we do not, their presence only on the south polar residual cap must relate to the physical differences between the caps. Probably this difference relates to the presence of dry-ice in the south polar cap and not in the north.

We propose that the flat floors of the basins and the fact that they appear to grow together only through radial growth is indicative of both an environment where wind transport of debris is low and/or where basin formation is rapid. As a result, we believe the basins indicate that the ice in the region where they are found is CO<sub>2</sub> ice, a medium that can rapidly ablate under south polar residual cap summer conditions.

The swiss-cheese terrain is visually similar to the topography of Canada Glacier where the basins are fairly randomly distributed (Fig. 4). Unlike the canyons seen on Taylor Glacier, which

are initiated by albedo differences resulting from the presence of medial moraines and therefore form features in linear arrays that are subsequently linked by water transport of debris, the Canada Glacier basins have no underlying linking mechanism. Similarly, we believe that unlike the Martian troughs, which we have proposed require wind removal of debris, both to prevent lag deposits from insulating the ice and preventing ablation and to link smaller features into elongated grooves, the Martian swiss-cheese basins, require fast growth or limited wind influence to explain why they are not linked into trough features.

If the swiss-cheese basins form in CO<sub>2</sub> ice, the basins walls could potentially ablate back on the order of a meter over the course of the summer (1-2 m of CO<sub>2</sub> frost sublimates off the south polar cap during the summer). Erosional widening of pits has been observed at the predicted rates (Malin et al. 2001), adding further support to inferences that these terrains are made of dry ice. Sublimation rates on the near-vertical walls of the swiss-cheese basins and on deposits at the foot of the scarps should be higher than sublimation from horizontal surfaces because near-vertical walls will capture more radiation, as discussed for the north polar cap in section 6. The debris contained in this ice would be deposited at the base of the wall, which could further enhance sublimation rates, thus creating moats, as observed near some scarps. However, this does not explain why fields of basins appear to maintain a relatively consistent depth. In the dry valleys, neighboring basins can be very different depths. This suggests that the depths of the Martian basins are controlled by an external mechanism such a change in ice composition.

## **9 Conclusions**

The dry valley glaciers in Antarctica appear to serve as a useful analogue for the Martian polar caps. Study of the basins and canyons seen on many dry valleys glacier provide us with insight

into the sequence of events necessary for the initiation and growth of large-scale features. Studying the dry valley glaciers also highlights the general processes required to maintain such features once they have formed. In particular, such comparison highlights the requirement of some mechanism to remove debris from the ice surface. Without such a mechanism, the debris can rapidly accumulate and insulate the ice from further sublimation. This implies that on Mars, there must be eolian removal of dust freed by sublimation from trough walls, which in turn indicates that the troughs are the result of some radiation and wind interaction.

Using the Pfeffer and Bretherton (1987) V-groove radiation model, adapted for Mars, our results indicate that, though the grooves on Martian ice sheets have a very large opening angle, there is still a significant increase in radiation absorption of the equator-facing wall. What is surprising, however, is that the large-scale grooves on the ice sheets have opening angles that are too wide to optimize solar absorption. We speculate that the reason for this inefficiency is that groove closure by ice flow overpowers solar-energy driven sublimation. This suggests that further work aimed at quantifying the energy absorption and sublimation within the grooves may allow us to estimate ice flow rates involved in the flow closure of the grooves, a topic we hope to address in future work.

Comparison of the Canada Glacier basins and the Martian south polar “swiss-cheese” terrain suggests that sublimation could be responsible for excavating the circular depressions seen. We believe the random distribution of the swiss-cheese basins indicates that wind removal of debris does not play a role in their development. We further suggest that this indicates that the basins form rapidly, perhaps indicating that the ice in which they are found is CO<sub>2</sub> ice. However, the consistent depth of basins over large areas indicates some mechanism of depth control such as a layer of “harder,” less volatile H<sub>2</sub>O or CO<sub>2</sub> clathrate ice.

## 10 References

- Budd, W.F., D. Janssen, J.H.I. Leach, I.N. Smith, and U. Radok, The north polar cap of Mars as a steady-state system, *Polarforschung* **56**, 43—63, 1986
- Byrne, S. and A. P. Ingersoll, Sublimation Model for Formation of Residual Cap Depressions. Abstract, Second Martian Polar Conference, Iceland, 2000.
- Clifford, S. M. et al., The state and future of Mars polar science and exploration, *Icarus*, **144** (2), 210—242, 2000.
- Durham, W. B., S. H. Kirby, and L. A. Stern, Effects of dispersed particulates on the rheology of water ice at planetary conditions, *J. Geophys. Res.*, **97**(20), 883-897, 1992.
- Durham, W. B., S. H. Kirby and L. A. Stern, Comparative rheologies of solid H<sub>2</sub>O, CO<sub>2</sub>, and CO<sub>2</sub> clathrate hydrate, Second Martian Polar Conference, Iceland, 2000.
- Farmer, C. B. and P.E. Doms, Global seasonal variation of water vapor on Mars and the implications for permafrost, *J. Geophys. Res.*, **84**, 2881—2888, 1979.
- Fisher, D. A., If Martian icecaps flow: Ablation mechanisms and appearance, *Icarus*, **105**, 501—511, 1993.
- Fisher, D. A., Internal layers in an “accublation” ice cap, a test for flow, *Icarus*, **144** (2), 289—294, 2000.
- Greve, R., Waxing and waning of the perennial north polar H<sub>2</sub>O ice cap of Mars over obliquity cycles, *Icarus* **144**, 419—431, 2000.
- Haberle, R. and B. Jakosky, Sublimation and transport of water from the north residual polar-cap on Mars, *J. Geophys. Res.*, **95**, 1423—1437, 1990.
- Howard, A. D., Origin of the stepped topography of the Martian poles, *Icarus*, **84**, 581—599, 1978.
- Howard, A. D., The role of Eolian processes in forming surface features of the martian polar layered deposits, *Icarus*, **144** (2), 267—288, 2000.
- Howard, A. D., J. A. Cutts and K. R. Blasius, Stratigraphic relationships within Martian polar cap deposits, *Icarus*, **50**, 161—215, 1982.
- Hvidberg, C. S., An ice flow model of the north polar Martian ice cap, Second Martian Polar Conference, Iceland, 2000.
- Ingersoll, A. P., Occurrence of liquid water, *Science*, **168**, 972—973, 1970.

- Ivanov, A. B. and D. O. Muhleman, The role of sublimation for the formation of the northern ice cap: results from the Mars Orbiter Laser Altimeter, *Icarus*, 144 (2), 436—448, 2000a.
- Ivanov, A. B. and D. O. Muhleman, Topography of the North and South Polar Ice Caps on Mars: Analysis of shape and troughs with a sublimation model, Second Martian Polar Conference, Iceland, 2000b.
- Jacob, M., *Heat Transfer, Volume II*, Wiley, New York, 1957.
- Jakosky, B. M. and R. M. Haberle, The seasonal behavior of water on Mars, in *Mars*, edited by. H. Kieffer, B. Jakosky, C. Snyder and M. Matthew, The University of Arizona press, 969—1016, 1992.
- Jakosky, B., B. Henderson and M. Mellon, The Mars water cycle at other epochs: Recent history of the polar caps and layered terrain, *Icarus*, 102, 286—297, 1993.
- Jakosky, B., B. Henderson and M. Mellon, Chaotic obliquity and the nature of the Martian climate, *J. Geophys. Res.*, 100(E1), 1579—1584, 1995.
- Jakosky, B.M.; Mellon, M.T.; Kieffer, H.H.; Christensen, P.R.; Varnes, E.S.; Lee, S.W., The thermal inertia of Mars from the Mars Global Surveyor Thermal Emission Spectrometer, *J. Geophys. Res.*, 105, 9643—9652, 2000.
- Kargel J.S. and J.I. Lunine, Clathrate hydrates on Earth and in the Solar System, in *Solar System Ices*, edited by B. Schmitt et al., Kluwer Academic, 97—117, 1998.
- Kargel, J.S., K.L. Tanaka, V.R. Baker, G. Komatsu, and D.R. MacAyeal, Formation and dissociation of clathrate hydrates on Mars: Polar caps, northern plains, and highlands. Houston, Texas, *Lunar Planet. Sci. XXXI*, abstract 1891 (CD-ROM), 2000.
- Kieffer, H. H., S. C. Chase Jr., T. Z. Martin, E. D. Miner, and F. D. Palluconi, Martian north pole summer temperatures: Dirty water ice, *Science*, 194, 1341—1343, 1976.
- Kieffer, H. H., Mars south polar spring and summer temperatures: A residual CO<sub>2</sub> frost, *J. Geophys. Res.*, 84, 8263—8288, 1979.
- Kieffer, H. H. and A. P. Zent, Quasi-periodic climate change on Mars, in *Mars*, edited by H.H. Kieffer et al., University of Arizona Press, Tucson, 1180—1220, 1992.
- Larsen, J., Modeling the northern remnant ice cap on Mars, Second Martian Polar Conference, Iceland, 2000.
- Larsen, J. and D. Dahl-Jensen, Interior Temperatures of the Northern Polar Cap on Mars, *Icarus*, 144, 456—462, 2000.

- Lewis, K. J., A. G. Fountain and G. L. Dana, Surface Energy Balance and Meltwater Production for a Dry Valley Glacier, Taylor Valley, Antarctica, *Annals of Glaciology*, 27, 603—609, 1998.
- Lewis, K. J., Solar-forced roughening of Antarctic glaciers and the Martian icecaps: How surficial debris and roughness affect glacial melting in Taylor Valley, Antarctica and how this can be applied to the Martian icecaps, PhD thesis, University of Colorado, Boulder, CO, 2002.
- Malin, M.C. and K.S. Edgett, Mass movement slope streaks imaged by the Mars Orbiter Camera, *J. Geophys. Res.*, 106, 23607—23633, 2001.
- Malin, M.C., M.A. Caplinger, and S.D. Davis, Observational evidence for an active surface reservoir of solid carbon dioxide on Mars, *Science* 294, 2146—2148, 2001.
- Mellon, M.T., Limits on the CO<sub>2</sub> content of the Martian polar deposits, *Icarus*, 124, 268—279, 1996.
- Nye, J., A flow model for the polar caps of Mars, *J. Glac.*, 46(154), 438—444, 2000.
- Paterson, W., *The Physics of Glaciers, 3rd Edition*, Elsevier Science, NY, 1994.
- Pfeffer, W. T. and C. S. Bretherton, The effect of crevasses on the solar heating of a glacier surface, in *The Physical Basis of Ice Sheet Modeling, IAHS Publ. no. 170*, edited by E. D. Waddington and J. S. Walder, 191—205, 1987.
- Ross, R.G. and J.S. Kargel, Thermal conductivity of Solar System ices, with special reference to Martian polar caps, in *Solar System Ices*, edited by B. Schmitt et al., Kluwer Academic, Dordrecht, 32—66, 1988.
- Schenk, P. and J. Moore. Web site, <http://www.lpi.usra.edu/research/msp/msp.html>
- Thomas, P. C., M. C. Malin, K. S. Edgett, M. H. Carr, W. K. Hartmann, A. P. Ingersoll, P. B. James, L. A. Sonderblom, J. Veverka and R. Sullivan, North-south geological differences between the residual polar caps on Mars, *Nature*, 404, 161—164, 2000.
- Thomas, P., S. Squyres, K. Herkenhoff, A. Howard and B. Murray, Polar deposits of Mars, in *Mars*, edited by H. Kieffer et al., The University of Arizona Press, 767—795, 1992.
- Toon, O. B., J. B. Pollack, W. Ward, J. A. Burns, and K. Bilshi, The astronomical theory of climatic change on Mars, *Icarus*, 44, 552—607, 1980.
- Zuber, M. T. et al., Observations of the North Polar Region of Mars from the Mars Orbiter Laser Altimeter, *Science*, 282, 2053—2060, 1988.

Figure 1: Mars Orbiter Camera (MOC) image of the Martian north (left image) and south (right image) polar regions during their respective summers. The central white area in each image is the residual cap. The north polar residual cap is roughly 1100 kilometers across and is cut by dark, spiral troughs; the south polar residual cap about 420 km across. MGS MOC Release No. MOC2-231, 22 May 2000 (left image); MGS MOC Release No. MOC2-225, 27 April 2000 (right image);]. Image Credit (these and other MOC images): NASA/JPL/Malin Space Science Systems. MOC images were obtained through the Malin Space Science Systems (MSSS) website, [http://www.msss.com/moc\\_gallery/](http://www.msss.com/moc_gallery/).

Figure 2: Cartoon representation of sublimation and accumulation on a scarp on the Martian icecap from Fisher, 1993.

Figure 3: Martian south polar residual cap "Swiss Cheese" terrain. MGS MOC Release No. MOC2-211, 8 March 2000. Image is illuminated by sunlight from the upper left. This image shows an upper layer of the Martian south polar residual cap that has been eroded, leaving flat-topped mesas into which are set circular depressions. The tallest mesas shown here stand about 4 meters high. Terrain such as this is found only on the south polar residual cap, leading to speculation that these landforms may result from the carbon dioxide ice thought to be common in the south polar region. The image covers an area 3 x 9 km near 85.6°S, 74.4°W at a resolution of 7.3 meters per pixel. This picture was taken during early southern spring on August 3, 1999.

Figure 4: Aerial photographs of the lower Canada Glacier. Top photo shows oblique view of several of the roughly circular basins. Photo is taken looking southwest; the asymmetry of the equator facing vertical wall and pole-facing, shallow slope can be seen. Bottom photo shows larger section of the glacier toe – the circular basins can be seen best in the lower right section of the image.

Figure 5: Lower Taylor Glacier, Taylor Valley, Antarctica. This image shows how the canyons at the glacier toe appear to be a continuation of banding in the ice seen far up-glacier. The section of glacier shown here is approximately 6 km long. North is toward the top of the image.

Figure 6: Canada and Taylor Glaciers, Taylor Valley, Antarctica. The large roughness features can be seen on the lower reaches of the glaciers. For scale, both glaciers are approximately 3 km wide.

Figure 7: Cross section profiles of troughs on the Martian north polar cap, derived from Mars orbiting laser altimeter (MOLA) data. Troughs of this nature are pervasive on the polar caps of both hemispheres. Note the scale shown here is exaggerated; the troughs are very shallow, with opening angles of up to 165°. Generally the equator-facing wall is twice as steep as the opposing wall, Fig. D being the most characteristic example.

Figure 8: Idealized V-groove geometry used in the analysis. The x- and y-coordinates refer to non-dimensional distances measured up the sides of the groove (both are 0 at the apex of the groove and 1 at the location where the groove wall intersects the flat surface into which the groove is cut). The angles  $\Psi$  and  $\gamma$  refer to the solar angle (described in the text) and the groove opening angle respectively. The angle  $\Psi$  is related to the solar zenith angle. The enhancement of solar absorption due to multiple diffuse reflections of the incoming solar beam is shown schematically. Also shown are the portions of the groove that are shadowed from the incoming solar beam and the portions that are illuminated directly. The opening angle  $\gamma$  depicted here is much smaller than for the typical grooves on the northern polar ice sheet of Mars (see Table 2).

Figure 9: Absorption by the V-groove geometry using  $\gamma=165^\circ$  and for local noon on the summer solstice at  $80^\circ\text{N}$ . See also Figures 2 and 3 of Pfeffer and Bretherton (1987) for further details and results applicable to terrestrial glaciers. Curves indicate the absorbed energy for the sun-facing and sun-opposing walls and for a flat surface.

Figure 10: Absorption by the V-groove geometry using  $\gamma=60^\circ$  and for local noon on the summer solstice at  $80^\circ\text{N}$ . Curves indicate the absorbed energy for the equator-facing and pole-facing walls and for a flat surface. The equator-facing wall is shadowed from the bottom of the groove to about  $y=0.44$ .

Table 1: Comparison of physical environmental parameters for the Antarctic dry valleys and Martian polar caps.

	Antarctic dry valleys	Martian north polar cap
Gravity	9.81 ms <sup>-2</sup>	3.72 ms <sup>-2</sup>
Solar constant (top of atmosphere)	1380 Wm <sup>-2</sup>	594 Wm <sup>-2</sup>
Atmospheric pressure	1000 mbar	5-20 mbar
Atmospheric water vapor pressure	0-9mbar	~10 <sup>-3</sup> mbar
Accumulation rates – CO <sub>2</sub> ice	none	1-2m/year (Zuber, 2000)
Accumulation rates – H <sub>2</sub> O ice	10 <sup>-2</sup> to 10 <sup>-1</sup> m water equivalent/year	10 <sup>-4</sup> m water equiv./year (Clifford et al., 2000)
Sublimation rates – CO <sub>2</sub> ice	none	1-2m/year (all overwinter accumulation sublimates)
Sublimation rates – H <sub>2</sub> O ice	10 <sup>-1</sup> m water equiv./year in ablation zone	10 <sup>-4</sup> to 10 <sup>-3</sup> m water equiv./year (Jakosky and Haberle, 1992)
Melt rates	10 <sup>-1</sup> to 10 <sup>0</sup> m water equiv./year ablation zone	none
Mean annual surface temperature	~255K	~155K (Clifford et al., 2000)
Flow speeds	10 <sup>0</sup> to 10 <sup>1</sup> m/year	order 10 <sup>-2</sup> m/year (Fisher, 2000)
Dust deposition rates	0.5-1 gm <sup>-2</sup> /year	20-200 g m <sup>-2</sup> /year (Thomas et al., 1992)
Volumetric fraction of debris in ice	<< 1%	1-50+% (Clifford et al., 2000)

Table 2: Parameters used to model the Martian insolation regime.

<b>Parameter</b>	<b>Value</b>	<b>Units</b>
Planetary Distance	1.524	A.U.
Obliquity	23.45	degrees
Length of Day	24.623	hours
Planetary Radius	3380	km
Solar Constant	594	Wm <sup>-2</sup>
Opening angle $\alpha$	165	degrees
Latitude	80 N	degrees

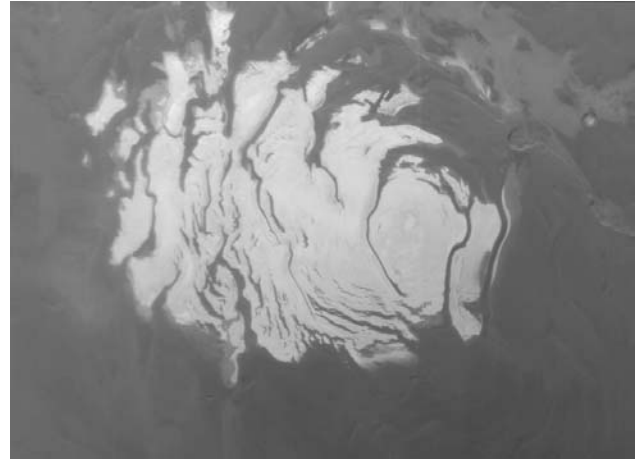
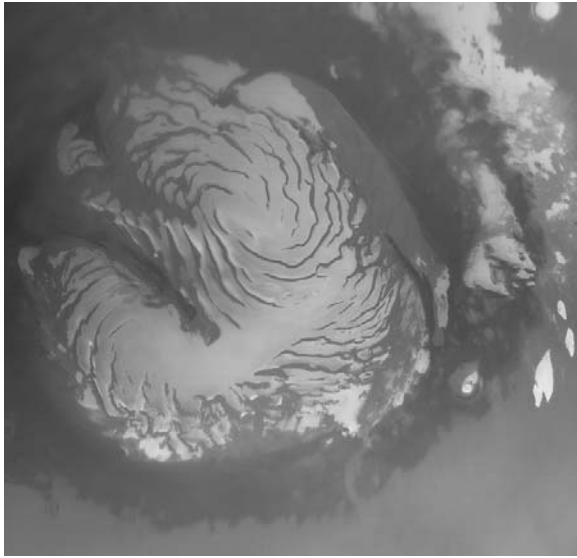


Figure 1: Mars Orbiter Camera (MOC) image of the Martian north (left image) and south (right image) polar regions during their respective summers. The central white area in each image is the residual cap. The north polar residual cap is roughly 1100 kilometers across and is cut by dark, spiral troughs; the south polar residual cap about 420 km across. MGS MOC Release No. MOC2-231, 22 May 2000 (left image); MGS MOC Release No. MOC2-225, 27 April 2000 (right image);]. Image Credit (these and other MOC images): NASA/JPL/Malin Space Science Systems. MOC images were obtained through the Malin Space Science Systems (MSSS) website, [http://www.msss.com/moc\\_gallery/](http://www.msss.com/moc_gallery/).

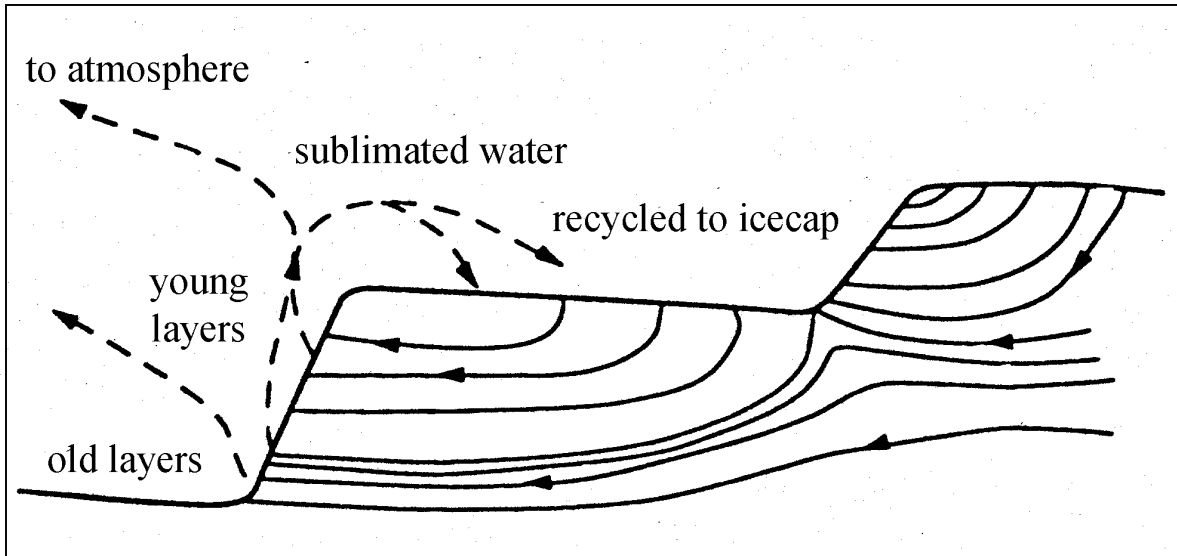


Figure 2: Cartoon representation of sublimation and accumulation on a scarp on the Martian icecap from Fisher, 1993.



Figure 3: Martian south polar residual cap "Swiss Cheese" terrain. MGS MOC Release No. MOC2-211, 8 March 2000. Image is illuminated by sunlight from the upper left. This image shows an upper layer of the Martian south polar residual cap that has been eroded, leaving flat-topped mesas into which are set circular depressions. The tallest mesas shown here stand about 4 meters high. Terrain such as this is found only on the south polar residual cap, leading to speculation that these landforms may result from the carbon dioxide ice thought to be common in the south polar region. The image covers an area 3 x 9 km near 85.6°S, 74.4°W at a resolution of 7.3 meters per pixel. This picture was taken during early southern spring on August 3, 1999.

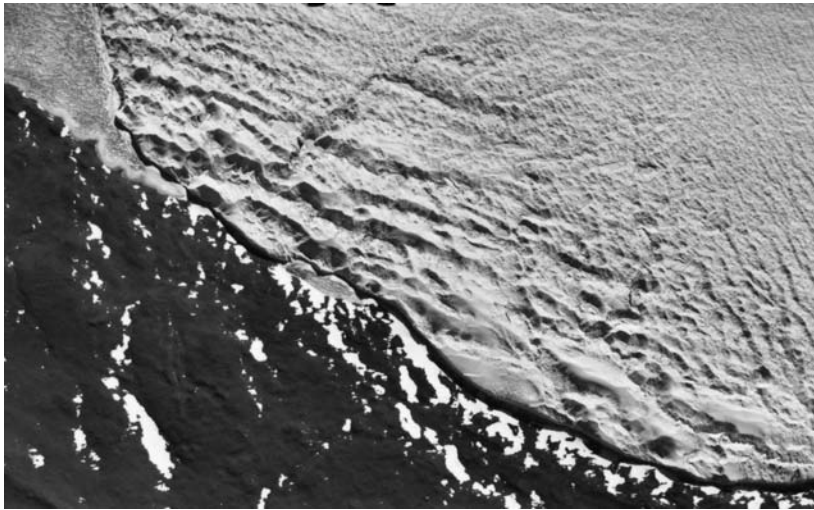
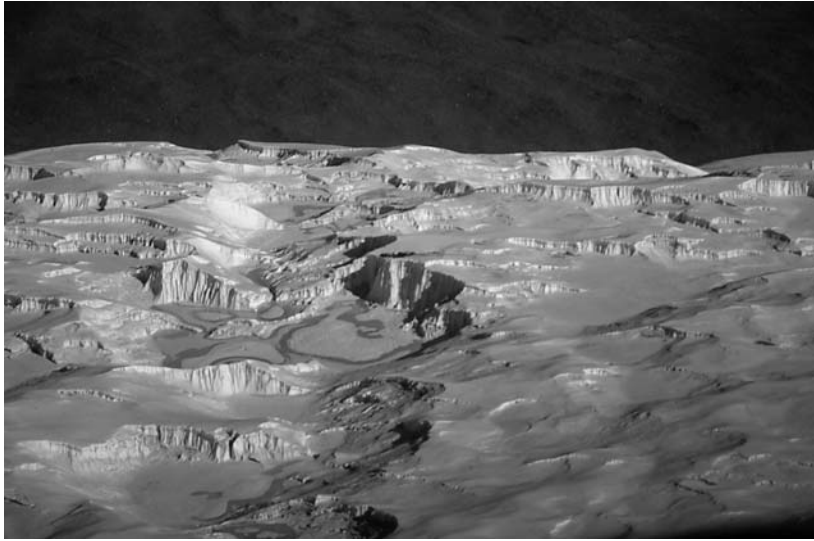


Figure 4: Aerial photographs of the lower Canada Glacier. Top photo shows oblique view of several of the roughly circular basins. Photo is taken looking southwest; the asymmetry of the equator facing vertical wall and pole-facing, shallow slope can be seen. Bottom photo shows larger section of the glacier toe – the circular basins can be seen best in the lower right section of the image.

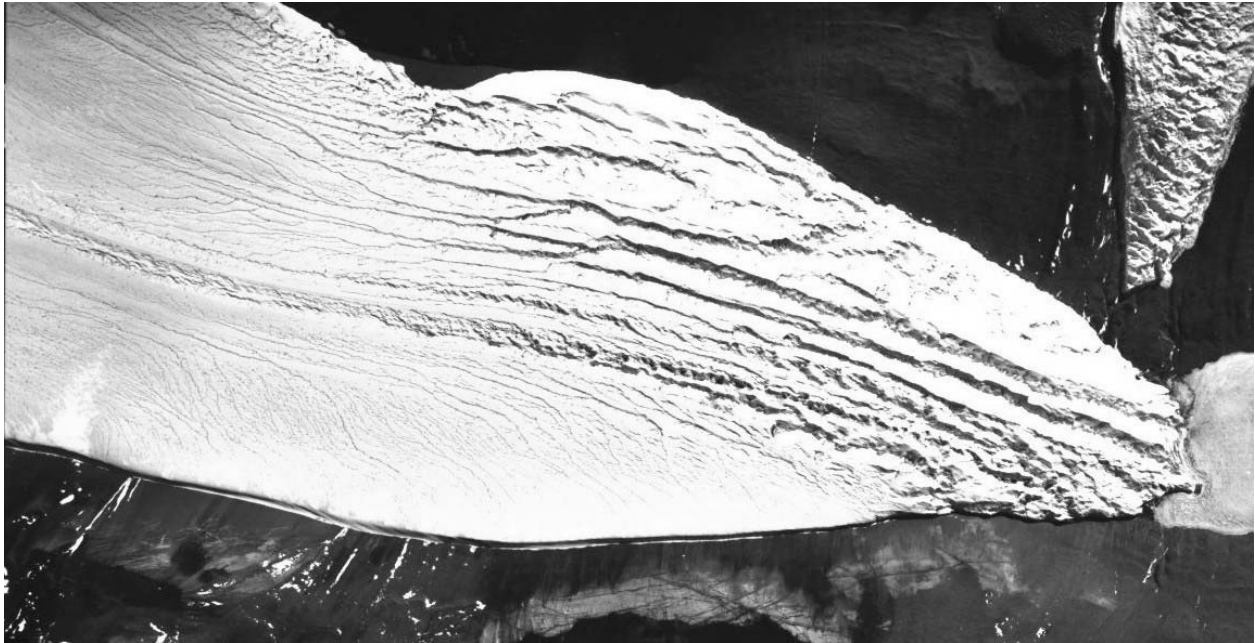


Figure 5: Lower Taylor Glacier, Taylor Valley, Antarctica. This image shows how the canyons at the glacier toe appear to be a continuation of banding in the ice seen far up-glacier. The section of glacier shown here is approximately 6 km long. North is toward the top of the image.



Figure 6: Canada and Taylor Glaciers, Taylor Valley, Antarctica. The large roughness features can be seen on the lower reaches of the glaciers. For scale, both glaciers are approximately 3 km wide.

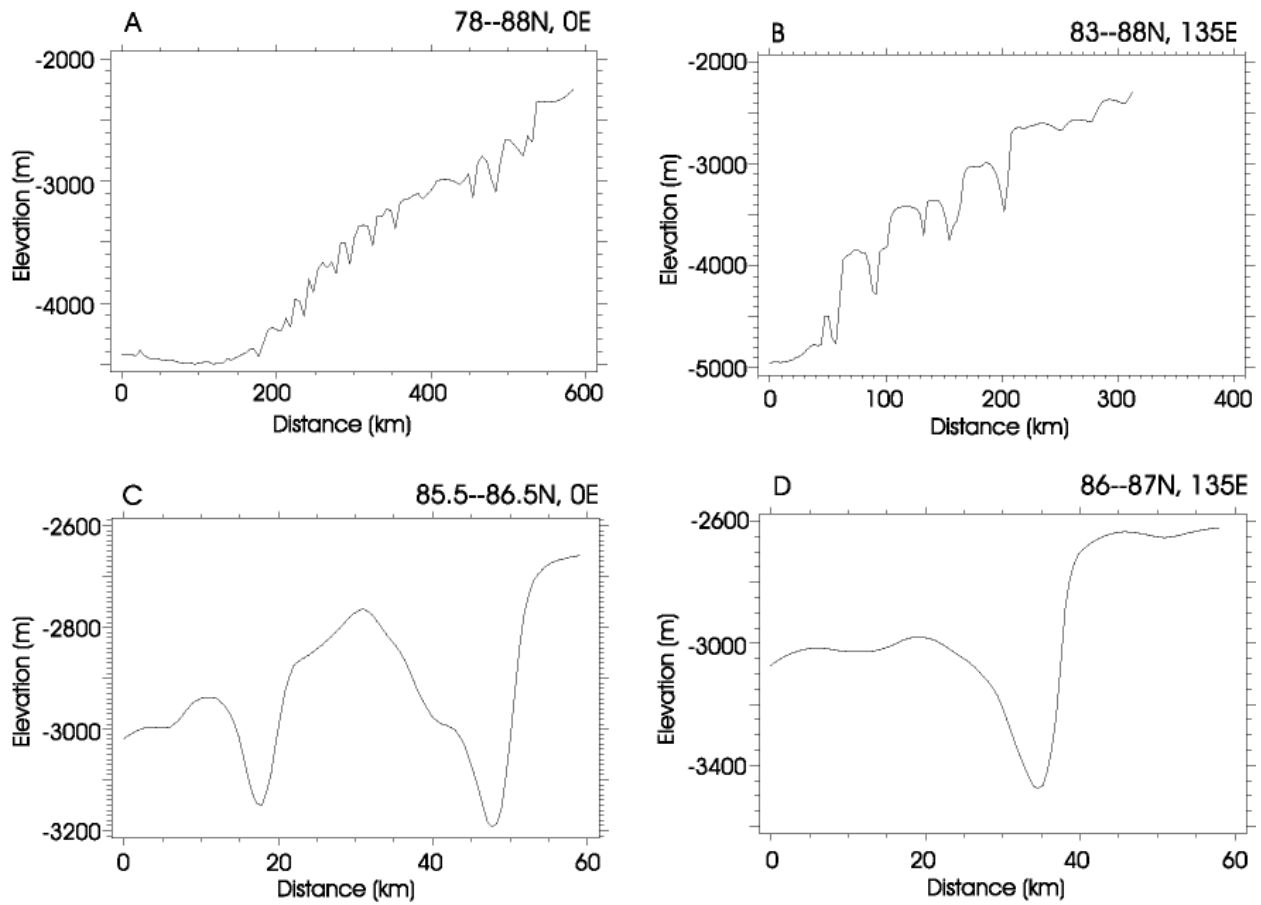


Figure 7: Cross section profiles of troughs on the Martian north polar cap, derived from Mars orbiting laser altimeter (MOLA) data. Troughs of this nature are pervasive on the polar caps of both hemispheres. Note the scale shown here is exaggerated; the troughs are very shallow, with opening angles of up to  $165^\circ$ . Generally the equator-facing wall is twice as steep as the opposing wall, Fig. D being the most characteristic example.

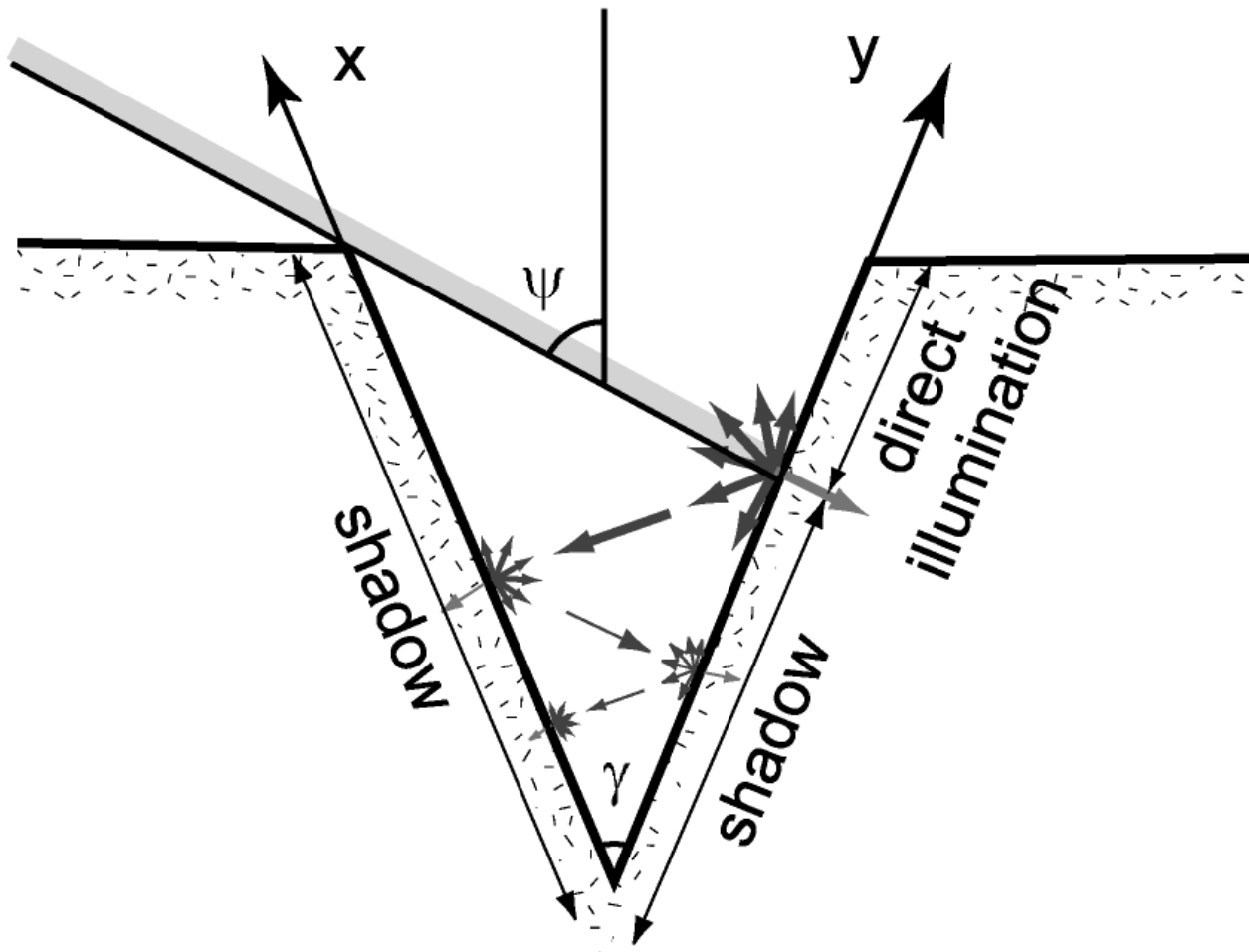


Figure 8: Idealized V-groove geometry used in the analysis. The x- and y-coordinates refer to non-dimensional distances measured up the sides of the groove (both are 0 at the apex of the groove and 1 at the location where the groove wall intersects the flat surface into which the groove is cut). The angles  $\Psi$  and  $\gamma$  refer to the solar angle (described in the text) and the groove opening angle respectively. The angle  $\Psi$  is related to the solar zenith angle. The enhancement of solar absorption due to multiple diffuse reflections of the incoming solar beam is shown schematically. Also shown are the portions of the groove that are shadowed from the incoming solar beam and the portions that are illuminated directly. The opening angle  $\gamma$  depicted here is much smaller than for the typical grooves on the northern polar ice sheet of Mars (see Table 2).

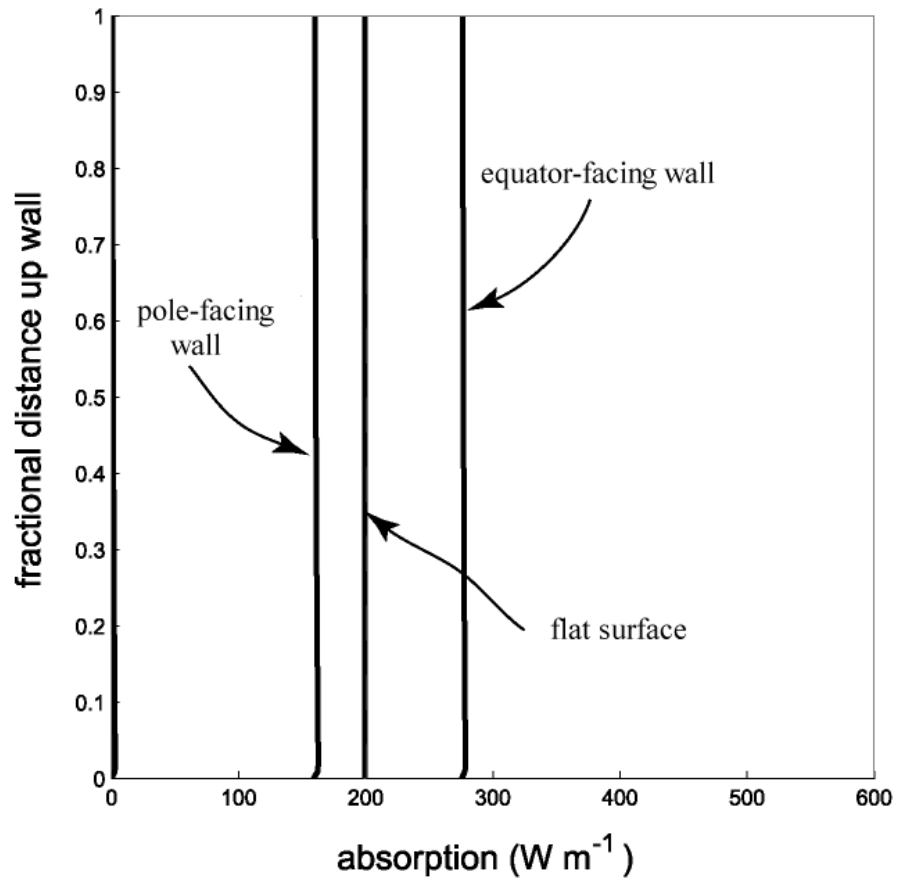


Figure 9: Absorption by the V-groove geometry using  $\gamma=165^\circ$  and for local noon on the summer solstice at  $80^\circ\text{N}$ . See also Figures 2 and 3 of Pfeffer and Bretherton (1987) for further details and results applicable to terrestrial glaciers. Curves indicate the absorbed energy for the sun-facing and sun-opposing walls and for a flat surface.

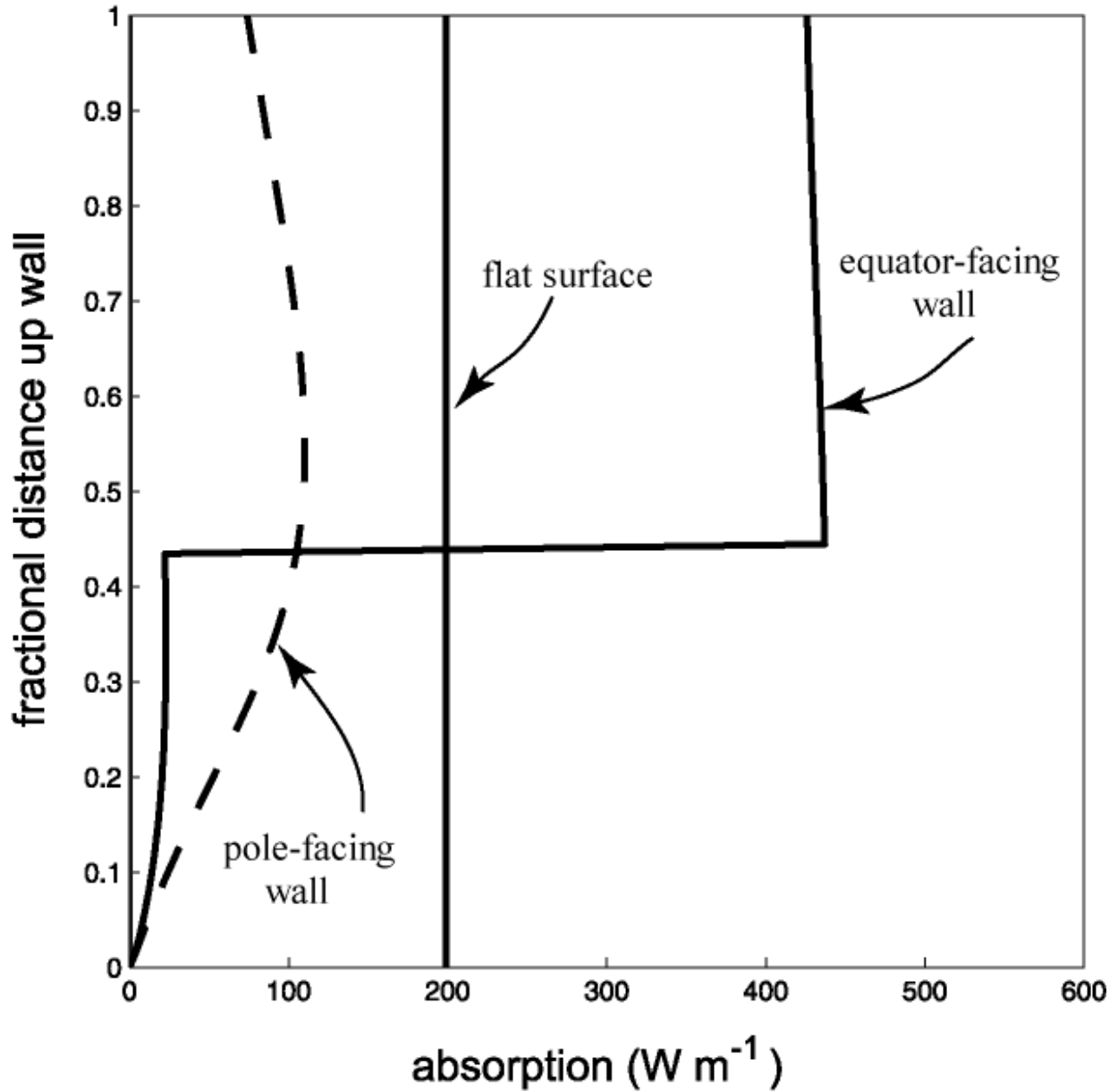


Figure 10: Absorption by the V-groove geometry using  $\gamma = 60^\circ$  and for local noon on the summer solstice at  $80^\circ\text{N}$ . Curves indicate the absorbed energy for the equator-facing and pole-facing walls and for a flat surface. The equator-facing wall is shadowed from the bottom of the groove to about  $y=0.44$ .